Characterization of the antimicrobial activity of the cell-penetrating peptide TAT-RasGAP$_{317-326}$

Maria Georgieva[2,&], Tytti Heinonen[1,&], Alessandra Vitale[3], Simone Hargraves[1], Senka Causevic[1], Trestan Pillonel[1], Leo Eberl[3], Christian Widmann[2,#], Nicolas Jacquier[1,#,*]

1. Institute of Microbiology, Lausanne University Hospital and University of Lausanne, Switzerland
2. Department of Physiology, University of Lausanne, Switzerland
3. Department of Plant and Microbial Biology, University of Zurich, Switzerland

& These authors contributed equally to this work

# These authors share senior authorship

Running title: Study of TAT-RasGAP$_{317-326}$ antimicrobial activity

Keywords: Antimicrobial peptide, anticancer peptide, antibiotic resistance, TAT-RasGAP$_{317-326}$, *Escherichia coli*, *Pseudomonas aeruginosa*

*Corresponding author:

Dr. Nicolas Jacquier, Institute of Microbiology, Department of Pathology and Laboratory Medicine, CHUV, Bugnon 48, CH-1011 Lausanne, Switzerland

Phone: +41213148539 ; Fax: +41213144060 ; Email : nicolas.jacquier@chuv.ch

Abstract

Antimicrobial peptides (AMPs) are molecules with antimicrobial activity and could be a promising alternative to classical antibiotics, whose clinical efficiency is undermined by emergence of resistance. Our group is studying one such antibiotic alternative – the antimicrobial peptide TAT-RasGAP$_{317-326}$. We recently reported the antimicrobial activity of this peptide against a range of Gram-positive and Gram-negative bacteria.

In this article, we show that the presence of divalent cations and low pH levels have an impact on TAT-RasGAP$_{317-326}$ activity, whereas serum proteins only partially reduce the antibacterial activity of TAT-RasGAP$_{317-326}$. In addition, we show that iron supplementation reduces TAT-RasGAP$_{317-326}$ binding to bacteria. Using a transcriptomics approach and screening of bacterial mutant libraries, we map the transcriptional response of bacteria when exposed to TAT-RasGAP$_{317-326}$ and identify cellular pathways that may play a role in bacterial resistance to TAT-RasGAP$_{317-326}$. We test combinations of TAT-RasGAP$_{317-326}$ with other AMPs and detect no evidence for an additive effect between any of the peptide combinations. Finally, we perform a resistance selection screen that reveals differences between bacterial strains with respect to their rate of resistance emergence against the TAT-RasGAP$_{317-326}$ peptide.

Taken together, our findings bring a better understanding of how extracellular factors might impact the antimicrobial activity of TAT-RasGAP$_{317-326}$ peptide and thus contribute basic biology insight into the mechanisms behind TAT-RasGAP$_{317-326}$ activity, potentially aiding future strategies to improve the efficiency of this peptide *in vivo*.

Introduction

The spread of antibiotic resistance in many bacterial species is severely limiting the benefits of antibiotics and a growing number of infections are becoming harder to treat [1]. The issue is further compounded by the shortage of new classes of antibiotics that could potentially compensate for the expanding resistance to standard antibiotics. Therefore, there is a need for the development of alternative antimicrobials that could be used in the clinic to treat bacterial infections. One group of such alternative antimicrobials are antimicrobial peptides (AMPs), several of which are already in clinical trials, with promising results as antibiotic alternatives [2].

AMPs are naturally occurring peptides produced in many different organisms [2]. In bacteria, AMP production confers an advantage to the producing strain in the colonization of ecological niches [3]. In multicellular organisms, AMPs such as human cathelicidin LL-37 and bovine bactenecin are generally a part of the innate immune system [4].

AMPs have several properties that make them attractive alternatives to antibiotics. These include their wide diversity, their relatively simple structure, and the possibility to bioengineer these peptides. Altogether, there are thousands of AMPs described in the literature and this diversity of AMPs is an attractive resource that may allow targeting a wide range of infections [5]. Indeed, there are examples of AMPs that can target both Gram-positive and Gram–negative bacteria [2]. Owing to their peptide nature, AMPs are amenable to bioengineering, which enables the targeted manipulation of the peptide gene (if naturally occurring) or complete chemical synthesis of the desired peptide. Such manipulations can increase peptide specificity and efficiency, as well as introduce favorable pharmacokinetic properties that would improve potential clinical application of the peptide.

AMPs are quite diverse, however, they possess a number of shared features. AMPs are usually short peptides consisting of 10-50 amino acids, display an overall positive charge and are rich in cationic and hydrophobic amino acids. While the mechanisms of action (MOA) of

AMPs against pathogens vary depending on the type of peptide, a common feature of the antimicrobial activity of AMPs seems to be the electrostatic interaction between the positively charged peptide and the negatively charged bacterial surface. For example, melittin, isolated from bee venom [6] and LL-37, part of the human innate immune system [7] have been shown to disrupt bacterial membrane integrity and cause pore formation [2]. Another AMP, the circularized polypeptide polymyxin B, derived from the Gram-positive bacterium *Bacillus polymyxa*, is also positively charged and able to permeabilize bacterial membranes [8].

For any antimicrobial with potential clinical application, we must consider the possibility of emergence of resistance. While rate of resistance to AMPs seems to be lower than the rate at which resistance to classic antibiotics arises, recent studies indicate that this process is more common than previously hypothesized, indicating that a careful evaluation of conditions favoring resistance towards AMPs is required prior to any systemic distribution of these compounds [9, 10]. It is thus essential to study not only the MOA of AMPs but also investigate any resistance mechanisms against them and thus define the best conditions that allow the safe use of these compounds.

Our group recently reported the discovery of the novel antimicrobial activity of the cell-penetrating peptide TAT-RasGAP$_{317-326}$, a cationic peptide of 22 amino acids. We showed its activity towards a broad spectrum of both Gram-positive and Gram-negative bacteria *in vitro* [11]. Initial studies on TAT-RasGAP$_{317-326}$ by our group highlighted its anticancer activity. We outlined its ability to both sensitize cancer cells to chemotherapy and directly kill cancer cells [12-16]. Previous research has shown that sensitization by this peptide occurs independently of caspases, apoptosis and necroptosis [14, 16], but requires p53 and PUMA [12]. Furthermore, we have identified that the WXW motif within the peptide sequence is required for both the anticancer and antimicrobial activities of TAT-RasGAP$_{317-326}$ [11, 17]. While we have begun to dissect the MOA of TAT-RasGAP$_{317-326,}$ we still lack a comprehensive understanding of the mechanisms behind its antimicrobial and anticancer effects.

Despite its potent *in vitro* antimicrobial activity, TAT-RasGAP$_{317-326}$ showed limited activity *in vivo* in a mouse model of *Escherichia coli* (*E. coli*) induced peritonitis [11]. This could be

due to environmental factors, such as binding to serum proteins, presence of chemicals or pH variations on the activity of TAT-RasGAP$_{317-326}$, as reported for other AMPs [18]. A better understanding of the MOA of TAT-RasGAP$_{317-326}$ and a careful investigation of factors influencing its activity would address this possibility. Insights from such investigations would also aid at developing strategies to improve the activity of this peptide *in vivo*, either through designing improved peptide-specific methods to deliver the peptide directly to the desired site of action or chemical modifications of the peptide itself to boost its activity. Altogether, these efforts will improve the potential of TAT-RasGAP$_{317-326}$ for the treatment of bacterial infections.

In this report, we studied the conditions required for TAT-RasGAP$_{317-326}$ to be efficient against bacteria in order to understand how we may improve the *in vivo* efficacy of this peptide. We first determined the effect of culture medium composition and pH levels on TAT-RasGAP$_{317-326}$ peptide activity. We then performed RNA sequencing (RNA-Seq) to investigate the transcriptional response of *E. coli* to the peptide. Finally, we assessed which pathways are required for TAT-RasGAP$_{317-326}$ activity by performing screenings of the Keio collection composed of *E. coli* single gene deletion mutants and of a *Pseudomonas aeruginosa* PA14 (*P. aeruginosa*) transposon mutant library.

We show that TAT-RasGAP$_{317-326}$ antibacterial activity is reduced in the presence of buffering compounds, low pH levels and high concentrations of divalent cations, but is unaffected by albumin. TAT-RasGAP$_{317-326}$ modifies the transcriptional landscape of *E. coli*, thereby inducing stress responses, especially through the activation of two-component systems, and altering the expression of several metabolic, membrane and ribosomal genes. Moreover, mutations affecting the two-component system repertoire increase sensitivity of bacteria to TAT-RasGAP$_{317-326}$ peptide. Because TAT-RasGAP$_{317-326}$ displays no additive effect with other AMPs we test here, it is likely TAT-RasGAP$_{317-326}$ and these AMPs have distinct MOAs. Finally, selection of strains resistant towards TAT-RasGAP$_{317-326}$ indicates that resistance to this peptide can occur and can lead to increased resistance to other AMPs. Taken together, these results provide a better understanding of the effects of TAT-RasGAP$_{317-}$

$_{326}$ on bacteria, which may open new research lines towards possible applications of TAT-RasGAP$_{317-326}$ peptide.

Results

Divalent cations in culture medium impact sensitivity of *E. coli* and *P. aeruginosa* to TAT-RasGAP$_{317-326}$ peptide

To investigate the antimicrobial properties of TAT-RasGAP$_{317-326}$, we studied the effect of the peptide on the two well-characterized laboratory strains *E. coli* MG1655 and *P. aeruginosa* PA14. First, we determined the minimal inhibitory concentrations (MICs) of TAT-RasGAP$_{317-326}$ peptide in LB medium for both *E. coli* and *P. aeruginosa* and determined these to be 8 μM and 32 μM respectively (Fig. 1A-B). Since *in vivo* conditions can vary regarding pH levels, nutrient availability, salt and protein concentrations, we investigated the effect of medium composition on the antimicrobial activity of the TAT-RasGAP$_{317-326}$ peptide. For both *E. coli* and *P. aeruginosa*, we measured MIC in BM2 medium containing either 2 mM (Mg^{high}) or 20 μM (Mg^{low}) $MgSO_4$ [19]. Interestingly, while MICs of both *E. coli* and *P. aeruginosa* were comparable between LB and BM2 Mg^{high} (Fig. 1C-D), we observed a drastic 8-times decrease of MIC in BM2 Mg^{low} medium (Fig. 1E-F). In contrast, low magnesium was reported to increase the MIC of polymyxin B, a well-described AMP, through induction of modifications of outer membrane composition and LPS structure in *P. aeruginosa* [20]. In line with these findings, we measured a 4-fold increase in polymyxin B MIC against *P. aeruginosa* but not *E. coli* in BM2 Mg^{low} medium compared to BM2 Mg^{high} (Fig. S1A-D). Taken together, these results indicate possible differences in the binding properties of TAT-RasGAP$_{317-326}$ to the bacterial surface in comparison to polymyxin B.

Because high magnesium concentration affects TAT-RasGAP$_{317-326}$ efficiency in BM2 medium, we hypothesized that a similar effect could be observed in complex LB medium supplemented with 2 mM $MgSO_4$. To address this hypothesis, we supplemented LB medium with 2 mM $MgSO_4$ and tested the antimicrobial activity of TAT-RasGAP$_{317-326}$ against *E. coli*

158 and *P. aeruginosa* in these conditions. In our experiments, magnesium supplementation
159 lowered the activity of TAT-RasGAP$_{317-326}$ against both *E. coli* and *P. aeruginosa* (Fig. S1E-
160 H). To determine whether the effect of high $MgSO_4$ concentration was caused by the presence
161 of magnesium ions, sulfate counter ions or rather due to a change in medium osmolarity, we
162 tested the activity of TAT-RasGAP$_{317-326}$ peptide in LB media supplemented with various salts.
163 We observed a similar drop in activity of the peptide in presence of 2 mM Mg^{2+}, Fe^{2+} or Ca^{2+},
164 both as sulfate and chloride salts (Fig. S2A-E). Ammonium sulfate did not affect the activity of
165 TAT-RasGAP$_{317-326}$ peptide (Fig. S2F), suggesting that the presence of divalent cations, but
166 not sulfate ions or changes in osmolarity have an effect on TAT-RasGAP$_{317-326}$ activity. To
167 quantify peptide uptake, we incubated bacteria with a FITC-labelled version of the peptide and
168 assessed fluorescent signal via flow cytometry. Addition of Trypan Blue (TB), an efficient
169 quencher of extracellular fluorescence, to the bacterial sample labelled with FITC-TAT-
170 RasGAP$_{317-326}$ revealed the specific accumulation of intracellular peptide. TB has been
171 demonstrated to quench the fluorescence of FITC-labelled compounds [21-23]. According to
172 its properties, TB is unable to pass the membrane of intact cells and is therefore unable to
173 quench intracellular fluorescence [24]. We verified this with bacteria incubated with FITC-
174 TAT-RasGAP$_{317-326}$ at 37°C, whose fluorescence was decreased but not completely abolished
175 after quenching with TB (Fig. 2G and 2H). In contrast, fluorescence of bacteria incubated with
176 FITC-TAT-RasGAP$_{317-326}$ on ice, a condition where entry is inhibited and only surface binding
177 occurs, is completely abolished after quenching with TB (Fig. 2G and 2H). Using this
178 experimental strategy, we showed that Fe^{2+} supplementation inhibited entry of the peptide
179 (Fig. S2G). In contrast, supplementation with Mg^{2+} or Ca^{2+} did not have effect on peptide
180 adhesion and entry (Fig. S2G).
181
182 **pH level and presence of buffering compounds in LB medium have an impact on TAT-**
183 **RasGAP$_{317-326}$ antimicrobial activity**
184 Besides salt concentration, pH levels can also vary across different *in vivo* conditions and
185 can influence the activity of AMPs [18]. To determine whether pH level of the culture medium

186 influences the activity of the TAT-RasGAP$_{317-326}$ peptide, we used the buffering compound 2-
187 (N-morpholino)ethanesulfonic acid (MES) [25] to create LB media with varying pH levels (pH
188 5.5, pH 6.0, pH 6.5 and pH 7.0). We confirmed that pH is stable in presence of buffering agent
189 (Table S1). We found that peptide activity against both *E. coli* and *P. aeruginosa* is reduced
190 at low pH (Fig. 2A-D and S3A-D). To address the possibility that low pH has an effect on TAT-
191 RasGAP$_{317-326}$ peptide integrity, we preincubated the peptide at pH 5.5 prior to testing its
192 activity against bacteria in LB medium pH 7.0. We found pre-incubation had no effect (Fig.
193 S4A), suggesting that the decreased activity of TAT-RasGAP$_{317-326}$ against bacteria in low pH
194 medium is due to a physiological adaptation of the bacteria and not to decreased peptide
195 stability. Intriguingly, we also found that peptide activity was reduced in LB medium buffered
196 with MES compared to non-buffered LB medium (Fig. 2D-E and S3D-E). This change might
197 depend on the buffering effect of MES or differences in the osmolarity of the media. To
198 determine whether a change in osmolarity is sufficient to affect peptide activity, we
199 supplemented LB with the non-metabolizable sugar sorbitol at same concentration as MES
200 (100 mM) but could not observe any effect on TAT-RasGAP$_{317-326}$ activity (Fig. 2F and S3F).
201 We then investigated the effect of pH on peptide binding using flow cytometry. We performed
202 this experiment on ice, which blocks entry of the peptide (Fig. 2H). We determined that
203 incubation at pH 5.5, but not addition of MES, lowered the binding of FITC-labelled TAT-
204 RasGAP$_{317-326}$ to *E. coli* cells (Fig. 2G). In addition, the proportion of bacteria showing
205 internalization of FITC-labelled TAT-RasGAP$_{317-326}$ was lower at pH 5.5 than at pH 7.0 (Fig.
206 S4B). The effect of medium buffering on peptide activity seems to be specific for TAT-
207 RasGAP$_{317-326}$, since the activity of polymyxin B was not affected by supplementation of
208 medium with MES (Fig. S3G-L). Interestingly, low pH affected the activity of polymyxin B on
209 *P. aeruginosa* (Fig. S3G), but had only a minor effect on *E. coli* sensitivity to polymyxin B (Fig.
210 S3J).
211
212 **Serum and albumin have a mild effect on the antimicrobial activity of TAT-RasGAP$_{317-326}$**
213

It has been previously reported that serum albumin can bind to AMPs and thus lower their activity *in vivo* [26, 27]. To examine the effect of albumin on TAT-RasGAP$_{317-326}$, we tested the activity of the peptide in the presence of either bovine serum albumin (BSA) or fetal calf serum (FCS) and compared this to TAT-RasGAP$_{317-326}$ activity alone. BSA and FCS moderately increased (2 to 4 times) the MIC of TAT-RasGAP$_{317-326}$ on *E. coli* (Table1). Melittin was inactive at the maximal tested concentration (256 μg/ml) in presence of 50% FCS or 50 mg/ml BSA. Our results indicate that the presence of albumin has a mild effect on the antimicrobial activity of TAT-RasGAP$_{317-326}$.

TAT-RasGAP$_{317-326}$ is bactericidal against *E. coli* and *P. aeruginosa*

Our measurements of the MIC of TAT-RasGAP$_{317-326}$ peptide (Fig. 1) are based on the optical density method, which measures culture turbidity associated directly with bacterial growth. However, the optical signal at OD_{600} measures turbidity due to both live bacteria as well as dead bacterial debris in the culture medium. Moreover, we may not be able to differentiate a bacteriostatic from a bactericidal agent using this technique, since both would block proliferation and would result in very low turbidity. To quantify the number of bacteria that survive incubation with TAT-RasGAP$_{317-326}$, we determined the number of colony-forming units in a bacterial culture exposed to peptide. For *E. coli*, we observed a stable number of surviving bacteria through the entire experiment with 10 μM of the peptide, which is consistent with the observation that this concentration is approximatively the MIC as determined by measuring the optical density. In contrast, a decrease in bacterial viability was observed at peptide concentrations higher than or equal to 15 μM, suggesting the peptide is bactericidal at these concentrations (Fig. 3A). We performed a similar experiment with *P. aeruginosa* in BM2 Mg^{low} medium where we observed growth inhibition and decreased bacterial viability at 1 μM and 2 μM TAT-RasGAP$_{317-326}$, respectively (Fig. 3B). Interestingly, TAT-RasGAP$_{317-326}$ peptide had slower time-kill kinetics against *E. coli* than polymyxin B, an antibacterial agent, which is known to act by membrane permeabilization [28] (Fig. 3C). Similarly, TAT-RasGAP$_{317-}$

241 $_{326}$ killed *P. aeruginosa* more slowly than polymyxin B (Fig. 3D). We determined that killing of
242 *E. coli* was accompanied by an accumulation of fluorescent TAT-RasGAP$_{317-326}$ peptide in the
243 cytosol (Fig. 3E) and by changes in bacterial morphology (Fig. 3F).
244
245 **TAT-RasGAP$_{317-326}$ alters the transcriptional landscape of *E. coli***
246 It has been previously shown that AMPs can have more than one target and may also
247 indirectly impact a number of cellular processes [29]. To assess the overall effect of TAT-
248 RasGAP$_{317-326}$ on the *E. coli* transcriptome, we performed RNA-Seq analysis and compared
249 the transcriptional profile of bacteria exposed to the TAT-RasGAP$_{317-326}$ peptide and of
250 untreated bacteria. For these experiments, we chose a concentration of peptide (10 μM) that
251 inhibits growth but is not bactericidal (Fig. 3A). Among the 4419 transcripts predicted from the
252 *E. coli* MG1655 genome, 95.6% (n = 4223) were detected for at least one of the conditions.
253 Figure 4A and Dataset1 present data for the fold change in gene expression between bacteria
254 incubated in the presence or absence of TAT-RasGAP$_{317-326}$ peptide as well as the average
255 level of expression for each gene. We excluded from our analysis genes whose expression
256 was below the threshold set at 16 reads per kilobase of transcripts per million reads (RPKM).
257 Overall, TAT-RasGAP$_{317-326}$ treatment notably affected the expression of 962 genes (fold
258 change > 4), 11.0% of these were upregulated (red dots in Fig. 4A, Table S2) while 11.8%
259 were downregulated (blue dots in Fig. 4A, Table S3).
260 We assessed and validated twelve genes from the RNA-Seq data by qRT-PCR on RNA
261 extracted under the same conditions as for the RNA-Seq analysis. Five of these were reported
262 as upregulated, five as downregulated and two as unchanged according to the RNA-seq
263 analysis. One of the unchanged genes, *ompR*, was used as the housekeeping reference gene
264 for normalization. We obtained good correlation between the fold changes obtained with RNA-
265 Seq and with qRT-PCR (Fig. 4B).
266 To determine which biological processes or pathways were over-represented among
267 differentially expressed genes, we performed KEGG pathway [30-32] and GO term analyses
268 [33, 34]. The analysis of KEGG pathways revealed that several metabolic and information-

processing pathways were enriched among differentially expressed genes (Fig. 4C-D). For example, seven of the eight genes responsible for enterobactin synthesis in *E. coli* (included in "biosynthesis of siderophore group nonribosomal peptides" KEGG pathway) were upregulated upon peptide treatment. Other metabolic pathways such as carbon metabolism (citrate cycle, pyruvate metabolism) and oxidative phosphorylation were downregulated. GO term analysis also highlights the metabolic changes induced by TAT-RasGAP$_{317-326}$ (Fig. S5). Functions related to stress response were activated, causing strong modifications of the transcription profiles of transporters and regulatory pathways.

Screening of the Keio *E. coli* deletion mutant library uncovers genes that regulate bacterial resistance to TAT-RasGAP$_{317-326}$ peptide

Since our results suggest that TAT-RasGAP$_{317-326}$ has a different MOA compared to described AMPs, we screened the Keio collection of *E. coli* deletion mutants [35] for genes whose deletion influences resistance to TAT-RasGAP$_{317-326}$. Each strain of the Keio collection was grown in presence of 5 μM TAT-RasGAP$_{317-326}$. This concentration of peptide does not kill wild-type *E. coli* over the course of 24 hours following peptide addition (Fig. 3A). OD_{590} was measured 1.5, 3, 6 and 24 hours after addition of TAT-RasGAP$_{317-326}$ (Dataset 2). We calculated the distribution of the fold change growth upon incubation with TAT-RasGAP$_{317-326}$ versus without peptide for each strain at 6h and 24h (Fig. 5A-B). Resistant strains were defined as growing more than the wild-type average plus two times the standard deviation at 6 hours (Fig. 5A). Hypersensitive strains were defined as growing less than the wild-type average minus three times the standard deviation 24 hours after addition of the peptide (Fig 5B). Using these thresholds, we selected 27 resistant (Table S4) and 356 hypersensitive strains (Table S5). While the wild-type strains grew slower in the presence than in the absence of TAT-RasGAP$_{317-326}$, resistant strains grew similarly in both conditions and hypersensitive strains showed no growth in the presence of the peptide (Fig. 5C). Results of this screening indicate that deletions of genes involved in carbon metabolism, citrate cycle, oxidative phosphorylation (carbon metabolism, citrate cycle, oxidative phosphorylation) sensitized bacteria to TAT-

297 RasGAP$_{317-326}$ peptide (Fig. 5D-E). We also found that some two-component systems and
298 transcriptional regulators are required to maintain a normal rate of resistance to the peptide
299 (Fig. 5D-E). Analysis of resistant mutants showed that they carry deletions in genes involved
300 in LPS biogenesis and oxidative phosphorylation (Table S4). Interestingly, deletion of *febP*,
301 involved in enterobactin import, caused an increase in resistance towards TAT-RasGAP$_{317-326}$
302 further indicating that iron uptake may play an important role in the activity of this peptide.
303
304 **Transposon screening in *P. aeruginosa***
305 Since TAT-RasGAP$_{317-326}$ is active against both *E. coli* and *P. aeruginosa*, we wanted to
306 investigate whether some of the pathways that play a role in resistance to the peptide are
307 shared between the two bacterial species. To do this analysis, we exposed a *P. aeruginosa*
308 transposon library to TAT-RasGAP$_{317-326}$ and identified mutants that showed hypersensitivity
309 to the peptide [36]. We grew this library in presence or absence of 0.5 μM TAT-RasGAP$_{317-326}$
310 for 12 generations and performed deep sequencing in order to detect mutants, which could
311 not proliferate compared to others (Dataset 3). We interpreted lack of proliferation of these
312 mutants as a read-out of hypersensitivity to TAT-RasGAP$_{317-326}$. We identified 75 genes,
313 whose disruption via transposon insertion caused increased sensitivity to the peptide (Table
314 S6). Interestingly, 26 of these (35%) are associated with hypersensitivity to other antimicrobial
315 peptides [36]. Some of these genes code for LPS modifying enzymes such as *arnA*, *arnB* and
316 *arnT*, and for two-component regulators such as *parS* and *parR* that are involved in the
317 regulation of LPS modification. Among the genes, in which transposon insertion caused
318 hypersensitivity towards TAT-RasGAP$_{317-326}$ and not towards other AMPs, we identified *algJ*,
319 *algK* and *algX*, genes of the biosynthesis pathway of the extracellular polysaccharide alginate.
320 We also observed that mutants in genes coding for the RND efflux transporter MdtABC and
321 CusC, a component of the trans-periplasmic Cu^+ transporter CusCFBA, appear to be
322 hypersensitive to TAT-RasGAP$_{317-326}$. Other pathways that seem to be important for TAT-
323 RasGAP$_{317-326}$ resistance are related to carbon metabolism, redox reactions and translation
324 regulation (Table S6).

We next compared the lists of hypersensitive strains found in screenings in *E. coli* and in *P. aeruginosa*. We identified 15 gene orthologues, whose disruption causes hypersensitivity to the TAT-RasGAP$_{317-326}$ peptide in both *E. coli* and *P. aeruginosa* (Table 2). Among them, five are coding for two-component system proteins: *parR* and *parS* (*rtsA* and *rstB* in *E. coli*), *phoP*, *pmrB* (*qseC* in *E. coli*) and *colR* (*cusR* in *E. coli*). These five mutants display hypersensitivity to polymyxin B in *P. aeruginosa* [36], indicating that adaptability through these regulatory pathways is required to respond to AMPs. We also found genes conserved between *P. aeruginosa* and *E. coli* that respond specifically to treatment with TAT-RasGAP$_{317-326}$ and are involved in diverse cellular processes such as transcriptional regulation, DNA repair, glyoxylate detoxification, redox reactions, transmembrane transport and LPS biosynthesis (Table 2).

Combining TAT-RasGAP$_{317-326}$ peptide and other AMPs does not produce additive effects.

In order to determine whether TAT-RasGAP$_{317-326}$ activity is additive with the action of other AMPs, we performed growth tests of *E. coli* in presence of different combinations of TAT-RasGAP$_{317-326}$, melittin, LL-37 and polymyxin B, using sub-inhibitory concentrations of each peptide (Fig. 6A). Sub-inhibitory concentrations were chosen so that addition of two times this concentration would cause a visible drop in bacterial proliferation (Fig. 6A vs 6B). The additive effect of these AMPs was then tested by measuring the growth of *E. coli* in presence of combinations of any two AMPs (Fig. S6). To assess additivity, we calculated percent growth after 6 h of treatment compared to untreated control (Fig. 6C). We did not observe additive effect for TAT-RasGAP$_{317-326}$ with the three other AMPs tested. However, there is an additive effect of the combination of melittin and polymyxin B (2.8% of growth), and the combination of LL-37 and polymyxin B (0.8% of growth). Notably, the combination of melittin and polymyxin B caused stronger growth inhibition (2.8%) than incubation with the individual double doses (77.3% for melittin and 63.8% for polymyxin B, Fig. 6C). This effect is reminiscent of the synergism previously reported between melittin and antibiotics such as doripenem and

353 ceftazidime [37]. In contrast, the combination of melittin and TAT-RasGAP$_{317-326}$ showed an
354 antagonist effect, since sub-inhibitory concentration of melittin blocked the growth inhibition
355 caused by the TAT-RasGAP$_{317-326}$ peptide (Fig. 6D). To better understand the cause of this
356 antagonistic effect, we performed FACS analysis using FITC-labelled TAT-RasGAP$_{317-326}$. We
357 found that, in presence of melittin, binding of FITC-labelled TAT-RasGAP$_{317-326}$ to *E. coli*
358 bacteria was not affected and is comparable to the control condition where bacteria were
359 incubated with FITC-labelled TAT-RasGAP$_{317-326}$ alone (Fig. 6E). However, entry of the
360 labelled version of TAT-RasGAP$_{317-326}$ peptide was inhibited in presence of melittin (Fig. 6F).
361
362 **Appearance of TAT-RasGAP$_{317-326}$ peptide-resistant strains**
363 One argument for the introduction of AMPs in the clinic as an antibiotic alternative is the
364 low rate of peptide resistance and the fact that low rate of cross-resistance to other AMPs or
365 antibiotics has been detected so far [9, 10, 38]. To address this topic, we tested the kinetics
366 of resistance towards TAT-RasGAP$_{317-326}$ peptide in several bacterial strains (*E. coli*, *P.*
367 *aeruginosa*, *S. aureus* and *S. capitis*). First, we grew our parent bacterial strains overnight in
368 presence of sub-inhibitory concentrations of the peptide. We then diluted this parent culture
369 into two subcultures, one of which was exposed to an increased concentration of the TAT-
370 RasGAP$_{317-326}$ peptide while the other was kept in the same concentration of peptide as the
371 parent culture. Once bacterial growth was detected in the culture exposed to an elevated
372 concentration of the peptide, the process was repeated thereby exposing the bacterial culture
373 to sequentially increasing concentrations of peptide for a total of 20 passages. For each
374 passage, we measured the corresponding MIC (Fig. 7). Using this approach, we obtained
375 strains with increased MICs for *E. coli*, *S. capitis* and *S. aureus*, but not *P. aeruginosa* (Fig. 7,
376 Table 3 and Tables S7-10). It should be noted that the parental strain of *S. aureus* has a
377 peptide MIC in the range 64-128 μM and this MIC rapidly increased to 256 μM (Table S10).
378 We did not expose bacteria to higher MIC values, as any higher concentration of peptide is
379 not soluble in culture medium. To test whether the strains recovered at passage 20 for *E. coli*
380 and passage 12 for *S. aureus* showed increased resistance to other AMPs as well, we

determined the fold change of the MICs for polymyxin B, melittin and LL-37 relative to the corresponding parental strains that did not undergo selection (Table 3). Interestingly, the resistant *E. coli* strain did not show increased MICs to the other AMPs we tested as compared to the parental strain. In contrast, *P. aeruginosa* selected for resistance to TAT-RasGAP$_{317-326}$ showed increased MIC towards other AMPs. Similar to *P. aeruginosa*, the *S. aureus* and *S. capitis* strains selected for resistance to TAT-RasGAP$_{317-326}$ exhibited increased MICs towards other AMPs (Table 3).

Discussion

AMPs are promising alternatives to classical antibiotics. One such alternative that our lab studies is the antimicrobial peptide TAT-RasGAP$_{317-326.}$ While we have recently reported the antimicrobial activity of TAT-RasGAP$_{317-326}$ against both Gram-positive and Gram-negative bacterial strains [11], we lack a comprehensive understanding of the mechanisms behind the mode of action of this peptide.

Here, we investigated the effects of salt concentration and pH levels on TAT-RasGAP$_{317-326}$ activity. We also studied the interplay between TAT-RasGAP$_{317-326}$ and other AMPs, and assessed the rate of emergence of TAT-RasGAP$_{317-326}$ resistance in various bacterial strains. We showed that TAT-RasGAP$_{317-326}$ activity depends on medium composition – specifically, salt concentration and pH levels. The divalent cations Mg^{2+} and Ca^{2+} lowered the activity of TAT-RasGAP$_{317-326}$, an effect that was even more pronounced with Fe^{2+}. We also determined that low pH affects peptide activity. Both pH levels and iron reduced the affinity of the peptide to bind to bacteria. This could be the result of iron binding to a putative target of TAT-RasGAP$_{317-326}$ on the bacterial surface, thereby blocking peptide accessibility to the bacterial surface. Low pH levels could be affecting overall charge of the bacterial cell envelope or modify the conformation or levels of putative peptide binding partners located on the bacterial surface, thus decreasing peptide binding to bacteria. In contrast to iron and low pH levels, magnesium and calcium did not block peptide binding and entry. However, peptide was less efficient at killing *E. coli* grown in LB medium supplemented with magnesium and calcium.

Potentially, these cations might induce a physiological response of the bacteria that increases resistance to the TAT-RasGAP$_{317-326}$ peptide.

To investigate the bacterial response to TAT-RasGAP$_{317-326}$, we performed RNA-Seq analysis of *E. coli* exposed to TAT-RasGAP$_{317-326}$. We measured a profound effect of the peptide on transcriptional regulation in bacteria exposed to peptide: 22.8 % of detected genes were differentially transcribed after peptide exposure. Stress response, metabolism, translation machinery as well as membrane transporters were strongly modulated. Notably, we also observed that genes involved in iron transport are strongly upregulated in the presence of the peptide.

In an attempt to further characterize the MOA of TAT-RasGAP$_{317-326}$, we screened the *E. coli* Keio deletion mutant collection as well as a *P. aeruginosa* transposon mutant library. These screening experiments revealed the importance of two-component systems and carbon metabolism in bacterial response to TAT-RasGAP$_{317-326}$ peptide. Notably, we detected peptide resistance in bacterial Keio strains deleted for genes involved in LPS biosynthesis, suggesting that interaction between LPS and TAT-RasGAP$_{317-326}$ peptide might be required for its antimicrobial activity. Moreover, mutations in genes coding for alginate biosynthesis in *P. aeruginosa* caused hypersensitivity towards TAT-RasGAP$_{317-326}$. Bacterial surface composition may thus be an important parameter for activity of TAT-RasGAP$_{317-326}$. It should be noted that deletion of *entB*, a gene coding for an enterobactin transporter, causes partial resistance towards the peptide in *E. coli*. This result, together with the protective effect of Fe^{2+}, highlights a possible role of iron receptors or transporters in the antimicrobial activity of TAT-RasGAP$_{317-326}$. Further work will be required to determine whether the iron transport system is involved in peptide translocation.

We observed that TAT-RasGAP$_{317-326}$ has no additivity with pore-forming AMPs. This is compatible with the hypothesis that TAT-RasGAP$_{317-326}$ does not have a pore-forming MOA. Moreover, this indicates that combinations of TAT-RasGAP$_{317-326}$ with other AMPs do not increase the activity of TAT-RasGAP$_{317-326}$. In contrast, we observed that melittin had a protective activity against TAT-RasGAP$_{317-326}$. We showed that melittin blocks the entry of

437 TAT-RasGAP$_{317-326}$, possibly by binding the bacterial membrane and not allowing TAT-
438 RasGAP$_{317-326}$ to translocate. Our results indicate that interactions between the AMPs tested
439 here are diverse and range from synergism (polymyxin B and melittin for example) to
440 antagonism (TAT-RasGAP$_{317-326}$ and melittin) and no effect (TAT-RasGAP$_{317-326}$ and
441 polymyxin B, for example).

442 Prior to clinical application of an antimicrobial peptide, it is important to determine the rate
443 at which resistance against this peptide might arise in bacteria. To investigate this question,
444 we performed selection of TAT-RasGAP$_{317-326}$-resistant mutants in *E. coli*, *S. capitis* and *S.*
445 *aureus*. *P. aeruginosa* resistant strains were selected in medium containing a concentration
446 of TAT-RasGAP$_{317-326}$ corresponding to 10 times the MIC. However, when we subsequently
447 tested these strains to determine MIC, we found they possessed only 2- to 4- fold increase in
448 MICs. We hypothesize that this discrepancy might be due to transient adaptations of *P.*
449 *aeruginosa* to TAT-RasGAP$_{317-326}$ during the resistance selection screen, which resulted in
450 higher apparent MIC. Taken together, these results indicate that resistance to TAT-
451 RasGAP$_{317-326}$ can appear to different extents in diverse bacteria. An *E. coli* strain that showed
452 resistance to TAT-RasGAP$_{317-326}$ was not resistant to other AMPs (Table 3). This was different
453 for resistant strains of *S. aureus* and *S. capitis*, which showed increased resistance to other
454 AMPs. This indicates that different mechanisms of resistance may be at play in different
455 bacterial species.

456 Overall, in this paper, we show the role of extracellular factors influencing the antimicrobial
457 activity of TAT-RasGAP$_{317-326}$, characterize the transcriptional response of bacteria to TAT-
458 RasGAP$_{317-326}$, outline the interplay between TAT-RasGAP$_{317-326}$ and other AMPs, and raise
459 awareness for emergence of peptide resistance in bacteria. Taken together, our findings will
460 contribute to a better understanding of the mechanisms underlying TAT-RasGAP$_{317-326}$ activity
461 and may provide future directions to improve the efficacy of this peptide *in vivo*.

462

463

Material and methods

Strains and growth conditions

E. coli strains K-12 MG1655 substrain or BW25113 were grown in LB or Basal Medium 2 (BM2; 62 mM potassium phosphate buffer [pH 7.0], 7 mM $(NH_4)_2SO_4$, 10 μM $FeSO_4$, 0.4% (wt/v) glucose and 0.5% tryptone) with high (2mM) or low (20 μM) concentration of Magnesium ($MgSO_4$) [39]. *Pseudomonas aeruginosa* strain PA14 was grown either in LB or BM2 medium. *Staphylococcus capitis* [11] and *S. aureus* (ATCC 29213) strains were grown in tryptic soy broth (TSB) [40]. All strains were stored at -80°C, in their respective medium, supplemented with ~25% glycerol. When required, antibiotics were added at final concentrations of 50 μg/mL (kanamycin), 20 μg/mL (gentamycin), or 100 μg/mL (carbenicillin). When indicated, LB was buffered with 100 mM of the buffering agent 2-(N-morpholino)ethanesulfonic acid (MES, Sigma-Aldrich, Saint-Louis, MO) and pH was adjusted with HCl [25]. 100 mM sorbitol (Sigma-Aldrich) was added to LB as an osmoprotectant when indicated. The retro-inverse TAT-$RasGAP_{317-326}$ peptide (amino acid sequence DTRLNTVWMWGGRRRQRRKKRG) and the N-terminal FITC-labelled version of this peptide were synthesized by SBS Genetech (Beijing, China) and stored at -20°C. Chemicals were purchased from Sigma-Aldrich, unless otherwise specified.

MIC measurements

The minimum inhibitory concentration (MIC) of peptide was defined as the lowest concentration of peptide that resulted in no visible growth. Overnight cultures were diluted to OD_{600} = 0.1 and grown with shaking at 37°C for one hour. MICs were measured by diluting these cultures (1:20 for LB and TSB cultures and 1:8 for BM2 cultures) and then adding 2-fold dilutions of the peptide (starting with 256 μM) in 96-well plates. Volume of media (with peptide) per well was 100 μl and 10 μl of diluted cultures were added to each well. Cell growth was monitored via OD_{600} measurement after overnight growth with shaking at 37°C. OD_{600} readings were measured by FLUOstar Omega microplate reader (BMG Labtech, Ortenberg, Germany).

Peptide-free growth control wells and bacteria-free contamination control wells were included. First concentration at which no bacterial growth could be detected was defined as the MIC.

CFU measurements

Overnight cultures were diluted to OD_{600} = 0.1 and grown with shaking at 37°C for one hour. MICs were measured by adding indicated concentrations of peptide or antibiotics to the culture tube (1 ml culture volume). Cell growth was monitored via OD_{600} measurement by Novaspec II Visible spectrophotometer (Pharmacia LKB Biotechnology, Cambridge, England) and colony forming units (CFU) assay. Each time point (two, four and six hours) was taken by removing 10 µl and performing 10-fold serial dilutions. Four dilutions of each condition were then plated in the absence of peptide and grown at 37°C overnight. CFU were measured by counting the resulting number of colonies the next day.

Confocal microscopy

Overnight cultures of *E. coli* MG1655 were diluted to OD_{600} = 0.1, incubated or not for one hour with 10 µM FITC-labelled TAT-$RasGAP_{317-326}$, stained with 5 µg/ml FM4-64 and fixed with 4% paraformaldehyde solution. Incubation with DAPI was subsequently performed and pictures were acquired on a LSM710 confocal microscope (Zeiss, Oberkochen, Germany). Images were analyzed with ImageJ software [41].

Electron microscopy

Bacteria were fixed with 2.5% glutaraldehyde solution (EMS, Hatfield, PA) in Phosphate Buffer (PB 0.1 M pH 7.4) for 1 hour at room temperature. Then, bacterial samples were fixed by incubating in a freshly prepared mix of 1% osmium tetroxide (EMS) and 1.5% potassium ferrocyanide in phosphate buffer for 1 hour at room temperature. The samples were then washed three times in distilled water and spun down in 2% low melting agarose, solidified on ice, cut into $1mm^3$ cubes and dehydrated in acetone solution at graded concentrations (30%-

518 40min; 50%-40min; 70%-40min; 100%-3x1h). This was followed by infiltration in Epon at
519 graded concentrations (Epon 1/3 acetone-2h; Epon 3/1 acetone-2h, Epon 1/1-4h; Epon 1/1-
520 12h) and finally polymerization for 48h at 60°C in a laboratory oven. Ultrathin sections of 50
521 nm were cut on a Leica Ultramicrotome (Leica Mikrosysteme GmbH, Vienna, Austria) and
522 placed on a copper slot grid 2x1mm (EMS) coated with a polystyrene film. The bacterial
523 sections were stained in 4% uranyl acetate for 10 minutes, rinsed several times with water,
524 then incubated in Reynolds lead citrate and finally rinsed several times with water before
525 imaging.

526 Micrographs (10x10 tiles) with a pixel size of 1.209 nm over an area of 40x40 µm were
527 taken with a transmission electron microscope Philips CM100 (Thermo Fisher Scientific,
528 Waltham, MA) at an acceleration voltage of 80kV with a TVIPS TemCam-F416 digital camera
529 (TVIPS GmbH, Gauting, Germany). Large montage alignments were performed using
530 Blendmont command-line program from the IMOD software [42] and treated with ImageJ
531 software.

532

533 **Flow cytometry**

534 Overnight cultures of *E. coli* MG1655 were diluted 1:100 and grown to mid exponential
535 phase (OD_{600} = 0.4-0.6) with shaking at 37°C. Each culture was then diluted to OD_{600} = 0.1,
536 grown with shaking at 37°C for one hour and then treated with 10 µM FITC-labelled peptide
537 for 1 hour. Following peptide treatment, bacterial cells were washed in 1X PBS and diluted 1:5
538 before acquisition on a CytoFLEX benchtop flow cytometer (Beckman Coulter). For each
539 sample, 10,000 events were collected and analysed. Extracellular fluorescence was quenched
540 by adding 200 µL of Trypan Blue (0.4%).

541

542 **RNA-Seq**

543 Overnight cultures of *E. coli* MG1655 were diluted to OD_{600} = 0.1 and grown with shaking
544 at 37°C for one hour to mid exponential phase (OD_{600} = 0.4-0.6). Cultures were then treated
545 with TAT-$RasGAP_{317-326}$ (10µM) or left untreated (negative control), and grown with shaking at

37°C for an additional hour. For RNA extraction, protocol 1 in the RNAprotect Bacteria Reagent Handbook (Enzymatic lysis of bacteria) was followed using the RNeasy Plus Mini Kit (Qiagen) plus home-prepared TE buffer (10 mM Tris-HCl, 1 mM EDTA, pH 8.0) containing 1 mg/mL lysozyme (AppliChem, Chicago, IL). In the last step, RNA was eluted in 30 µL RNase-free water. Next, any contaminating DNA was removed using the DNA-free™ DNA Removal Kit (Invitrogen, Carlsbad, CA). 10x DNase buffer was added to the 30 µL eluted RNA with 2 µL rDNase I. This mix was incubated for 30 min at 37°C followed by rDNase I inactivation with 7 µL DNase Inactivation Reagent for 2 min with shaking (700 rpm) at room temperature. Samples were then centrifuged for 90 seconds at 10,000 x *g*, supernatant was transferred to a new tube, and stored at -80°C. Integrity of the samples was verified using the Standard Sensitivity RNA Analysis kit (Advanced Analytical, Ankeny, IA) with the Fragment Analyser Automated CE System (Labgene Scientific, Châtel-Saint-Denis, Switzerland). Samples that met RNA-Seq requirements were further processed and sent for sequencing. Preparation of the libraries and Illumina HiSeq platform (1x50 bp) sequencing were performed by Fasteris (Plan-les-Ouates, Switzerland). Raw reads were trimmed with trimmomatic version 0.36 [43] (parameters: ILLUMINACLIP: NexteraPE-PE.fa:3:25:6, LEADING: 28, TRAILING: 28 MINLEN: 30). Trimmed reads were mapped to the genome of *E. coli* K-12 MG1655 (accession: NC_000913.3) with bwa mem version 0.7.17 (https://arxiv.org/abs/1303.3997) using default parameters. Htseq version 0.11.2 [44] was used to count reads aligned to each gene (parameters: --stranded=no -t gene). Normalized expression values were calculated as Reads Per Kilobase of transcript per Million mapped reads (RPKM) with edgeR [45].

Keio collection screening

Deletion mutants from the Keio collection [35, 46] were used. Overnight cultures were diluted 1:100 in LB medium. Bacteria were incubated at 37°C with shaking for 1h before adding TAT-RasGAP$_{317-326}$ (5 µM final concentration). Plates were incubated statically at 37°C and OD_{590} was measured at 0h, 1.5h, 3h, 6h and 24h with FLUOstar Omega plate reader (BMG

Labtech, Ortenberg, Germany). Measurements were combined and analysed with R (version 3.6.1, [47]. Data analysis and visualisation were performed respectively with the *dplyr* (version 0.8.5) and *ggplot2* (version 3.3.0) packages from the *tidyverse* (version 1.3.0) environment. Since starting OD_{590} varied between strains, the corresponding starting value (T0 measurement) was subtracted at each measurement. Then, for each strain, the growth with TAT-$RasGAP_{317-326}$ was divided by the growth without peptide for normalization. The threshold for resistance was set based on normalized growth at 6h (NG6h) as 'NG6h strain' > 'NG6h WT + 2 x SD(NG6h WT)'. Hypersensitive strains were selected based on NG at 24h (NG24h) as 'NG24h strain' < 'NG24h WT – 3 x SD (NG24h WT)'.

Gene ontology (GO) annotation [34] was obtained from GO database (2020-09-01, "http://current.geneontology.org/annotations") and assigned to the list of gene deletion inducing hypersensitivity with the GO.db package (version 3.10.0 [48]). GO IDs were assigned to each gene and the corresponding GO names were obtained with the "Term" function. Additionally, the same set of genes was subjected to KEGG pathways analysis [30] with the KEGGREST package (version 1.26.1). Briefly, the KEGG orthology (KO) and KEGG pathway annotation were obtained from the KEGG database [32] for *E. coli* K-12 MG1655 (eco). The code is available on Github (https://github.com/njacquie/TAT-RasGAP_project).

Pseudomonas aeruginosa **PA14 transposon library screening**

The library of transposon (Tn) mutants in *P. aeruginosa* PA14 [36] was grown in BM2 supplemented with 20 µM $MgSO_4$ [39] and 0.2 % L-rhamnose monohydrate (Sigma-Aldrich, Ref. 83650) in the absence or presence of 0.5 µM TAT-$RasGAP_{317-326}$. Following growth for 12 generations, genomic DNA (gDNA) was extracted with the GenElute Bacterial Genomic DNA Kit (Sigma-Aldrich, Cat. No. NA2100-1KT). The transposon sequencing (Tn-seq) circle method [49, 50] was employed to sequence the transposon junctions. Briefly, the gDNA was sheared to an average size of 300 bp fragments with a focused-ultrasonicator. The DNA fragments were repaired and ligated to adapters with the NEBNext Ultra II DNA Library Prep Kit for Illumina (New England Biolabs). Following restriction of the Tn with BamHI (New

England Biolabs), the fragments were circularized by ligation and exonuclease treatment was applied to remove undesired non-circularized DNAs [49]. The Tn junctions were PCR amplified and amplicons were sequenced with the MiSeq Reagent Kit v2, 300-cycles (Illumina).

Following sequencing, the adapter sequences of the reads (.fastq) were trimmed with the command line "cutadapt -a adapter -q quality -o output.fastq.gz input.fastq.gz" [51]. The software Tn-Seq Explorer [52] mapped the trimmed and paired reads onto the *P. aeruginosa* UCBPP-PA14 genome [53], and determined the unique insertion density (UID, i.e. the number of unique Tn insertions divided per the length of the gene). The normalized UID between the treated and non-treated samples were compared and this ratio (log2-fold change, FC) was used to identify resistant determinants (log2-FC < - 1.0 and normalized UID > 0.0045).

Selection of resistant mutants

Bacteria were grown in the corresponding medium, diluted 1:100 and cultured overnight with 0.5x MIC of TAT-RasGAP$_{317-326}$. The subculture was diluted 1:100 and incubated with 0.5x or 1x MIC overnight. Cells that successfully grew were diluted 1:100 in medium containing the same concentration or twice the concentration of peptide. Each dilution in fresh medium containing peptide is considered one passage. This process was repeated for up to 20 passages.

Authorship

MG, TH, NJ, AV, SH and SC performed experiments. MG, TH, LE, CW and NJ were involved in the planning of the project and discussed the results. MG, TH, NJ and TP analysed the results. MG and NJ wrote the manuscript. All the authors proofread the manuscript.

Acknowlegments

We would like to thank Sébastien Aeby for technical support, Valentin Scherz for support in bioinformatics analyses and Prof. Gilbert Greub for sharing equipment and laboratories. This study was supported by an interdisciplinary grant of the Faculty of Biology and Medicine of the University of Lausanne.

Conflicts of interest

The authors declare no conflicts of interest.

References

1. O'Neill, J., *Tackling Drug-resistant Infections Globally: Final Report and Recommendations of the Review on Antimicrobial Resistance*, H. Government, Editor. 2016: London.
2. Kumar, P., J.N. Kizhakkedathu, and S.K. Straus, *Antimicrobial Peptides: Diversity, Mechanism of Action and Strategies to Improve the Activity and Biocompatibility In Vivo.* Biomolecules, 2018. **8**(1).
3. Hassan, M., et al., *Natural antimicrobial peptides from bacteria: characteristics and potential applications to fight against antibiotic resistance.* J Appl Microbiol, 2012. **113**(4): p. 723-36.
4. Xhindoli, D., et al., *The human cathelicidin LL-37--A pore-forming antibacterial peptide and host-cell modulator.* Biochim Biophys Acta, 2016. **1858**(3): p. 546-66.
5. Wang, G., X. Li, and Z. Wang, *APD3: the antimicrobial peptide database as a tool for research and education.* Nucleic Acids Res, 2016. **44**(D1): p. D1087-93.
6. Hong, J., et al., *How Melittin Inserts into Cell Membrane: Conformational Changes, Inter-Peptide Cooperation, and Disturbance on the Membrane.* Molecules, 2019. **24**(9).
7. Mendez-Samperio, P., *The human cathelicidin hCAP18/LL-37: a multifunctional peptide involved in mycobacterial infections.* Peptides, 2010. **31**(9): p. 1791-8.
8. Srinivas, P. and K. Rivard, *Polymyxin Resistance in Gram-negative Pathogens.* Curr Infect Dis Rep, 2017. **19**(11): p. 38.
9. Spohn, R., et al., *Integrated evolutionary analysis reveals antimicrobial peptides with limited resistance.* Nat Commun, 2019. **10**(1): p. 4538.
10. Lazzaro, B.P., M. Zasloff, and J. Rolff, *Antimicrobial peptides: Application informed by evolution.* Science, 2020. **368**(6490).
11. Heulot, M., et al., *The Anticancer Peptide TAT-RasGAP317-326 Exerts Broad Antimicrobial Activity.* Front Microbiol, 2017. **8**: p. 994.
12. Michod, D. and C. Widmann, *TAT-RasGAP317-326 requires p53 and PUMA to sensitize tumor cells to genotoxins.* Mol Cancer Res, 2007. **5**(5): p. 497-507.
13. Pittet, O., et al., *Effect of the TAT-RasGAP(317-326) peptide on apoptosis of human malignant mesothelioma cells and fibroblasts exposed to meso-tetra-hydroxyphenyl-chlorin and light.* J Photochem Photobiol B, 2007. **88**(1): p. 29-35.
14. Annibaldi, A., et al., *TAT-RasGAP317-326-mediated tumor cell death sensitization can occur independently of Bax and Bak.* Apoptosis, 2014. **19**(4): p. 719-33.
15. Chevalier, N., N. Gross, and C. Widmann, *Assessment of the chemosensitizing activity of TAT-RasGAP317-326 in childhood cancers.* PLoS One, 2015. **10**(3): p. e0120487.
16. Heulot, M., et al., *The TAT-RasGAP317-326 anti-cancer peptide can kill in a caspase-, apoptosis-, and necroptosis-independent manner.* Oncotarget, 2016. **7**(39): p. 64342-64359.
17. Barras, D., et al., *A WXW motif is required for the anticancer activity of the TAT-RasGAP317-326 peptide.* J Biol Chem, 2014. **289**(34): p. 23701-11.
18. Walkenhorst, W.F., *Using adjuvants and environmental factors to modulate the activity of antimicrobial peptides.* Biochim Biophys Acta, 2016. **1858**(5): p. 926-35.
19. Fernandez, L., et al., *Characterization of the polymyxin B resistome of Pseudomonas aeruginosa.* Antimicrob Agents Chemother, 2013. **57**(1): p. 110-9.
20. Macfarlane, E.L., et al., *PhoP-PhoQ homologues in Pseudomonas aeruginosa regulate expression of the outer-membrane protein OprH and polymyxin B resistance.* Mol Microbiol, 1999. **34**(2): p. 305-16.
21. Sahlin, S., J. Hed, and I. Rundquist, *Differentiation between attached and ingested immune complexes by a fluorescence quenching cytofluorometric assay.* J Immunol Methods, 1983. **60**(1-2): p. 115-24.
22. Loike, J.D. and S.C. Silverstein, *A fluorescence quenching technique using trypan blue to differentiate between attached and ingested glutaraldehyde-fixed red blood cells in phagocytosing murine macrophages.* J Immunol Methods, 1983. **57**(1-3): p. 373-9.
23. Jevprasesphant, R., et al., *Transport of dendrimer nanocarriers through epithelial cells via the transcellular route.* J Control Release, 2004. **97**(2): p. 259-67.
24. Wan, C.P., C.S. Park, and B.H. Lau, *A rapid and simple microfluorometric phagocytosis assay.* J Immunol Methods, 1993. **162**(1): p. 1-7.
25. Ma, Z., et al., *GadE (YhiE) activates glutamate decarboxylase-dependent acid resistance in Escherichia coli K-12.* Molecular Microbiology, 2003. **49**(5): p. 1309-1320.
26. Svenson, J., et al., *Albumin binding of short cationic antimicrobial micropeptides and its influence on the in vitro bactericidal effect.* J Med Chem, 2007. **50**(14): p. 3334-9.

27. Findlay, B., G.G. Zhanel, and F. Schweizer, *Investigating the antimicrobial peptide 'window of activity' using cationic lipopeptides with hydrocarbon and fluorinated tails.* Int J Antimicrob Agents, 2012. **40**(1): p. 36-42.
28. Daugelavicius, R., E. Bakiene, and D.H. Bamford, *Stages of polymyxin B interaction with the Escherichia coli cell envelope.* Antimicrob Agents Chemother, 2000. **44**(11): p. 2969-78.
29. Brazas, M.D. and R.E. Hancock, *Using microarray gene signatures to elucidate mechanisms of antibiotic action and resistance.* Drug Discov Today, 2005. **10**(18): p. 1245-52.
30. Kanehisa, M. and S. Goto, *KEGG: kyoto encyclopedia of genes and genomes.* Nucleic Acids Res, 2000. **28**(1): p. 27-30.
31. Kanehisa, M., et al., *New approach for understanding genome variations in KEGG.* Nucleic Acids Res, 2019. **47**(D1): p. D590-D595.
32. Kanehisa, M., *Toward understanding the origin and evolution of cellular organisms.* Protein Sci, 2019. **28**(11): p. 1947-1951.
33. Ashburner, M., et al., *Gene ontology: tool for the unification of biology. The Gene Ontology Consortium.* Nat Genet, 2000. **25**(1): p. 25-9.
34. The Gene Ontology, C., *The Gene Ontology Resource: 20 years and still GOing strong.* Nucleic Acids Res, 2019. **47**(D1): p. D330-D338.
35. Baba, T., et al., *Construction of Escherichia coli K-12 in-frame, single-gene knockout mutants: the Keio collection.* Mol Syst Biol, 2006. **2**: p. 2006 0008.
36. Vitale, A., et al., *Identification of Genes Required for Resistance to Peptidomimetic Antibiotics by Transposon Sequencing.* Front Microbiol, 2020. **11**: p. 1681.
37. Akbari, R., et al., *Highly Synergistic Effects of Melittin with Conventional Antibiotics Against Multidrug-Resistant Isolates of Acinetobacter baumannii and Pseudomonas aeruginosa.* Microb Drug Resist, 2019. **25**(2): p. 193-202.
38. Lazar, V., et al., *Antibiotic-resistant bacteria show widespread collateral sensitivity to antimicrobial peptides.* Nat Microbiol, 2018. **3**(6): p. 718-731.
39. Fernandez, L., et al., *The two-component system CprRS senses cationic peptides and triggers adaptive resistance in Pseudomonas aeruginosa independently of ParRS.* Antimicrob Agents Chemother, 2012. **56**(12): p. 6212-22.
40. Missiakas, D.M. and O. Schneewind, *Growth and laboratory maintenance of Staphylococcus aureus.* Curr Protoc Microbiol, 2013. **Chapter 9**: p. Unit 9C 1.
41. Schneider, C.A., W.S. Rasband, and K.W. Eliceiri, *NIH Image to ImageJ: 25 years of image analysis.* Nat Methods, 2012. **9**(7): p. 671-5.
42. Kremer, J.R., D.N. Mastronarde, and J.R. McIntosh, *Computer visualization of three-dimensional image data using IMOD.* J Struct Biol, 1996. **116**(1): p. 71-6.
43. Bolger, A.M., M. Lohse, and B. Usadel, *Trimmomatic: a flexible trimmer for Illumina sequence data.* Bioinformatics, 2014. **30**(15): p. 2114-20.
44. Anders, S., P.T. Pyl, and W. Huber, *HTSeq--a Python framework to work with high-throughput sequencing data.* Bioinformatics, 2015. **31**(2): p. 166-9.
45. Robinson, M.D., D.J. McCarthy, and G.K. Smyth, *edgeR: a Bioconductor package for differential expression analysis of digital gene expression data.* Bioinformatics, 2010. **26**(1): p. 139-40.
46. Yamamoto, N., et al., *Update on the Keio collection of Escherichia coli single-gene deletion mutants.* Mol Syst Biol, 2009. **5**: p. 335.
47. Team, R.C., *R: A language and environment for statistical computing. .* 2019.
48. Carslon, M., *GO.db: A set of annotation maps describing the entire Gene Ontology.* 2019.
49. Gallagher, L.A., J. Shendure, and C. Manoil, *Genome-scale identification of resistance functions in Pseudomonas aeruginosa using Tn-seq.* mBio, 2011. **2**(1): p. e00315-10.
50. Gallagher, L.A., et al., *Sequence-defined transposon mutant library of Burkholderia thailandensis.* mBio, 2013. **4**(6): p. e00604-13.
51. Martin, M., *Cutadapt removes adapter sequences from high-throughput sequencing reads.* EMBnet.journal, 2011. **17**: p. 10-12.
52. Solaimanpour, S., F. Sarmiento, and J. Mrazek, *Tn-seq explorer: a tool for analysis of high-throughput sequencing data of transposon mutant libraries.* PLoS One, 2015. **10**(5): p. e0126070.
53. Winsor, G.L., et al., *Enhanced annotations and features for comparing thousands of Pseudomonas genomes in the Pseudomonas genome database.* Nucleic Acids Res, 2016. **44**(D1): p. D646-53.

Tables:

	LB	12.5 % FCS	25 % FCS	50 % FCS	12.5 mg/ml BSA	25 mg/ml BSA	50 mg/ml BSA
TATRasGAP$_{317-326}$ (µM)	8	16-32	32	16	8	16-32	8-32
Melittin (µg/ml)	64-128	128-256	256	**>256**	256	**>256**	**>256**

Table 1: MIC of TAT-RasGAP$_{317-326}$ on *E. coli* MG1655 is increased by 2-4 fold in presence of serum or albumin. *E. coli* MG1655 was grown in LB overnight, diluted to 0.1 OD_{600} and grown for 1h. Culture was then diluted 20 times and 10 µl was added per well of a 96-well plate containing serial dilutions of TAT-RasGAP$_{317-326}$ or melittin in presence of the indicated quantities of fetal calf serum (FCS) or bovine serum albumin (BSA). The plate was then incubated at 37°C for 16 hours and MICs were quantified by turbidity measurement in 96 well plates. MIC was defined at the lowest AMP concentration that totally inhibited growth. Range of results of three independent experiments is indicated. When no range is indicated, all experiments performed gave the same result.

765

locus_tag	gene_symbol	description	Category	log2(FC_BM2vsTATRasGAP)	Hypersensitivity to PolB	E. coli homologues	Keio screening
PA14_41260	parR	two-component response regulator	Two-component regulator system	-4.268533546	Yes	rstA	Hypersensitive (2/2)
PA14_41270	parS	two-component sensor	Two-component regulator system	Inf	Yes	rstB	Hypersensitive (2/2)
PA14_49180	phoP	two-component response regulator PhoP	Two-component regulator system	Inf	Yes	phoP	Hypersensitive (2/2)
PA14_56950	colR	two-component response regulator	Two-component regulator system	Inf	Yes	cusR	More sensitive (1/2)
PA14_63160	pmrB	PmrB: two-component regulator system signal sensor kinase PmrB	Two-component regulator system	-3.492272393	Yes	qseC	Hypersensitive (2/2)
PA14_02390		transcriptional regulator	Transcription regulation	-5.436478184		cynR	Hypersensitive (2/2)
PA14_04160		transcriptional regulator	Transcription regulation	-1.231246313		yjiK	Hypersensitive (1/2)
PA14_70450	rpoZ	DNA-directed RNA polymerase subunit omega	Transcription regulation	-1.69421829		rpoZ	Hypersensitive (2/2)
PA14_65200	rnr	exoribonuclease RNase R	Translation regulation	-1.623618886		rnr	More sensitive (1/2)
PA14_18330	arnT	4-amino-4-deoxy-L-arabinose transferase	LPS biosynthesis	Inf	Yes	arnT	More sensitive (1/2)
PA14_71970	wbpW	GDP-mannose pyrophosphorylase	LPS biosynthesis	-4.335647742		cpsB	Hypersensitive (2/2)
PA14_18690		peroxidase	Oxido-reduction	-1.121328621		ahpC	More sensitive (1/2)
PA14_31920	opmB	outer membrane protein	Transmembrane transport	-5.044160761		cusC	More sensitive (1/2)
PA14_42700	alkA	DNA-3-methyladenine glycosidase II	DNA repair	-1.276606847		alkA	Hypersensitive (1/2)
PA14_52890		ring-cleaving dioxygenase	Antibiotic resistance	-1.036324267		gloA	Hypersensitive (1/2)

766

767 **Table 2: Genes found as more sensitive in both *P. aeruginosa* by transposon library**
768 **screening and in *E. coli* by Keio collection screening.** List of the genes, which mutants
769 were found as sensitive in transposon library screening in *P. aeruginosa* and whose
770 orthologues in *E. coli* were detected as sensitive in Keio collection screening. Transposon
771 mutants of *P. aeruginosa* were incubated in presence or absence of 0.5 μM TAT-RasGAP$_{317-326}$
772 in BM2 Mg^{low} medium for 12 generations. Transposon junctions were amplified and
773 sequenced. Fold change (FC) between abundance of transposon mutants with incubation in
774 absence (BM2) or presence (TATRasGAP) of the peptide was calculated and values are
775 presented as Log_2 of the FC. Inf indicates that no mutant was detected upon peptide treatment,
776 so Log_2 of the FC could not be calculated. Results obtained in a former study using the same

777 transposon library indicate that some gene mutations cause also hypersensitivity to polymyxin
778 B [36]. Ratio in Keio screening column indicates whether sensitivity was detected in both
779 deletion mutants of the collection (2/2) or only with one (1/2).

780
781
782
783
784

	TAT-RasGAP$_{317-326}$	Polymyxin B	Melittin	LL-37
E. coli	16	0.5	0.5	0.5
P. aeruginosa	4	2	>2	n.d.
S. capitis	32	>2	2	n.d.
S. aureus	>4	n.d.	8	n.d.

785

786 **Table 3: MICs of TAT-RasGAP$_{317-326}$-resistant strains towards other AMPs.** Fold
787 change of MICs between the original strains (*E. coli* MG1655, *P. aeruginosa* PA14, *S. capitis*
788 and *S. aureus* ATCC 29213) and strains exposed to increasing concentrations of TAT-
789 RasGAP$_{317-326}$ for 20 passages. MICs were measured as described for Fig. 1. n.d.: not
790 determined: MIC of the strain could not be determined.

791

Figure legends:

Figure 1: *E. coli* MG1655 and *P. aeruginosa* PA14 sensitivity to TAT-RasGAP$_{317-326}$ varies depending on the growth medium used. *E. coli* MG1655 was grown overnight in the indicated medium, diluted to 0.1 OD_{600} and grown for 1h. Culture was then diluted 20 times and 10 µl was added per well of a 96-well plate containing serial dilutions of TAT-RasGAP$_{317-326}$. OD_{600} measurements after 16 hours of incubation in presence of the indicated concentrations of TAT-RasGAP$_{317-326}$ are shown and MIC is defined as the lowest concentration of TAT-RasGAP$_{317-326}$ that completely inhibits bacterial proliferation. IC_{50} is defined as the concentration required to inhibit 50 % of growth and was calculated using GraphPad Prism 8. Indicated strains were grown overnight and diluted respectively in LB **(A-B)**, BM2 with 2mM $MgSO_4$ (Mg^{low}) **(C-D)** or BM2 with 20 µM $MgSO_4$ (Mg^{high}) **(E-F)**.

Figure 2: Low pH and high buffering capacities of medium differently affect activity of TAT-RasGAP$_{317-326}$. A-F) *E. coli* MG1655 was grown overnight at 37°C in LB medium containing 100 mM MES at the indicated pH (A-D), non-buffered LB at pH 7 (E) or LB supplemented with 100 mM sorbitol (F). Cultures were diluted to 0.1 OD_{600} in the same medium and grown one hour at 37°C before addition or not of the indicated concentrations of TAT-RasGAP$_{317-326}$. OD_{600} was measured at the indicated time points. **G)** *E. coli* MG1655 were treated as in (A-F) and FITC-labelled TAT-RasGAP$_{317-326}$ was added either at 37°C or on ice. Fluorescence was then quantified using flow cytometry. MFI: geometric mean of fluorescence intensity. Control are unlabeled bacteria. **H)** FITC signal after quenching with Trypan Blue.

Figure 3: TAT-RasGAP$_{317-326}$ is bactericidal against *E. coli* and *P. aeruginosa*. A-D) Overnight cultures of *E. coli* MG1655 in LB (A-B) and *P. aeruginosa* PA14 in BM2 Mg^{low} (C-D) were diluted to 0.1 OD_{600}. Peptide was added at the indicated concentrations 1 hour after dilution. Samples were taken at the indicated time points, serially diluted 10-fold in fresh LB

and plated on LB agar plates. Number of colony forming unit per ml (CFU/ml) of original culture was calculated. **E)** *E. coli* MG1655 strain was incubated for one hour with or without 10 μM FITC-labelled TAT-RasGAP$_{317-326}$. The bacterial sample was then labelled with 5 μg/ml FM4-64 and fixed with 4% paraformaldehyde solution. Incubation with DAPI was subsequently performed. Pictures were taken with a Zeiss LSM710 confocal microscope and analyzed using ImageJ software. **F)** *E. coli* bacteria treated as in (E) were fixed using glutaraldehyde and prepared for electron microscopy as described in Material and Methods section. Samples were imaged using transmission electron microscopy. Images were analyzed using ImageJ software.

Figure 4: TAT-RasGAP$_{317-326}$ remodels the transcriptional landscape of *E. coli*. RNA-seq analysis was performed on E. coli grown for 1h in the presence or absence of TAT-RasGAP$_{317-326}$. **A**) MA-plot of the average gene expression (x-axis, RPKM: read per kilobase million) vs the differential expression (y-axis). Threshold for gene expression is indicate with the blue horizontal line. The red lines indicate the limits for upregulated (red dots) and downregulated (blue dots) genes. **B**) Correlation between RNA-seq (log_2 Fold Change) and qRT-PCR (log_2 Relative Quantification) differential expression for a set of genes. **C-D)** Fraction of KEGG pathway genes that are upregulated (B) or downregulated (C) after treatment with TAT-RasGAP$_{317-326}$. Dot size indicates the number of genes in the selection.

Figure 5: Selection of hypersensitive and resistant *E. coli* deletion strains from KEIO collection. Single gene deletion strains were grown in LB medium with or without 5 μM TAT-RasGAP$_{317-326}$ and OD_{590} was measured at 0, 1.5, 3, 6, and 24 hours. **A-B**) Distribution of the fold change of the normalised growth (NG) with TAT-RasGAP$_{317-326}$ vs without peptide at 6h (A) and 24h (B). The mean of the wild-type strain and the standard deviation (SD) are indicated with the vertical solid and dashed lines, respectively. Arrows indicate the strains selected as resistant, hypersensitive and more sensitive. **C**) Growth curves of wild-type

(n=270), hypersensitive (n=356) and resistant (n=20) strains. Data are mean ± SD. **D**) Top 10 most represented KEGG pathways among hypersensitive strains. The number of hypersenstive strains in each pathway was normalised to the number of KEIO collection strains in the corresponding pathway. **E**) Biological processes GO term enrichment analysis with the 10 most represented terms among the hypersensitive strains.

Figure 6: TAT-RasGAP$_{317-326}$ shows no synergism with melittin, LL-37 and polymyxin B. *E. coli* MG1655 was grown overnight, diluted to 0.1 OD_{600}, and grown further during one hour before addition of the indicated AMPs. OD_{600} was measured at 2, 4 and 6h. For each AMP, two concentrations were tested: **(A)** a non-inhibitory concentration and **(B)** an inhibitory concentration corresponding to twice that of panel A. **C)** Combinations of AMPs were then tested and growth at 6h was expressed as percentage of growth compared to an untreated control. **D)** Sub-inhibitory concentration of melittin interfered with TAT-RasGAP$_{317-326}$ activity. Indicated AMPs were added and OD_{600} was measured as in (A). **E)** Bacteria were treated as in (A), but FITC-labelled TAT-RasGAP$_{317-326}$ was added and flow cytometry was performed in the indicated conditions. MFI: geometric mean of fluorescence intensity. Control are unlabeled bacteria. **F)** FITC signal after quenching with Trypan Blue.

Figure 7: Bacterial resistance against TAT-RasGAP$_{317-326}$ appears after selection with subinhibitory concentrations of peptide. The indicated strains were incubated in presence or absence of 0.5 MIC of TAT-RasGAP$_{317-326}$. Cultures were then diluted each day in medium containing either the same concentration of the peptide or double the concentration. Once bacterial growth was detected in the culture exposed to an elevated concentration of the peptide, the process was repeated thereby exposing the bacterial culture to sequentially increasing concentrations of peptide for a total of 20 passages. MIC of each passage was then measured and is presented as a fold change compared to the MIC of the original strain.

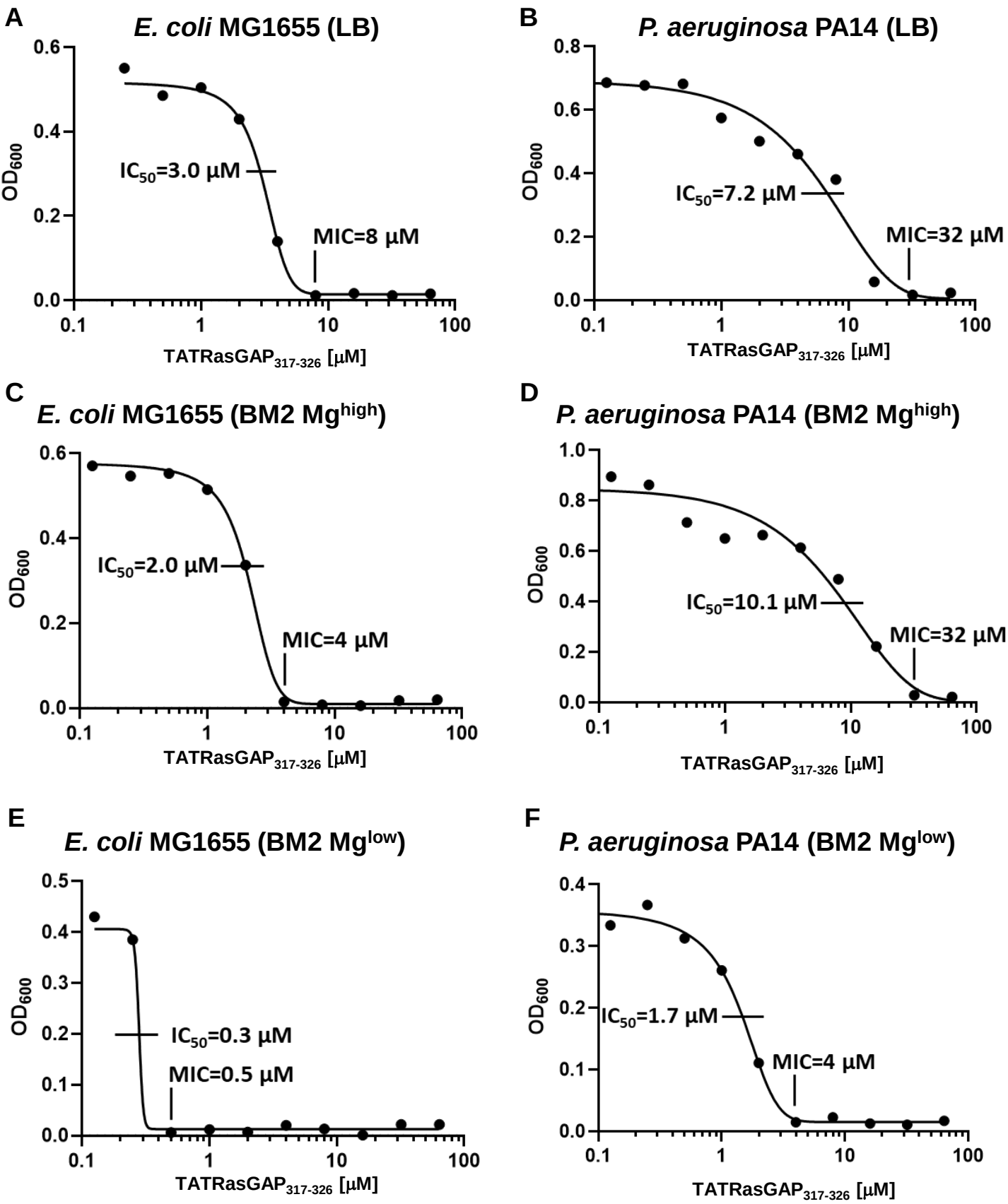

Figure 1: *E. coli* MG1655 and *P. aeruginosa* PA14 sensitivity to TAT-RasGAP$_{317-326}$ varies depending on the growth medium used. *E. coli* MG1655 was grown overnight in the indicated medium, diluted to 0.1 OD_{600} and grown for 1h. Culture was then diluted 20 times and 10 µl was added per well of a 96-well plate containing serial dilutions of TAT-RasGAP$_{317-326}$. OD_{600} measurements after 16 hours of incubation in presence of the indicated concentrations of TAT-RasGAP$_{317-326}$ are shown and MIC is defined as the lowest concentration of TAT-RasGAP$_{317-326}$ that completely inhibits bacterial proliferation. IC_{50} is defined as the concentration required to inhibit 50 % of growth and was calculated using GraphPad Prism 8. Indicated strains were grown overnight and diluted respectively in LB **(A-B)**, BM2 with 2mM $MgSO_4$ (Mg^{low}) **(C-D)** or BM2 with 20 µM $MgSO_4$ (Mg^{high}) **(E-F)**.

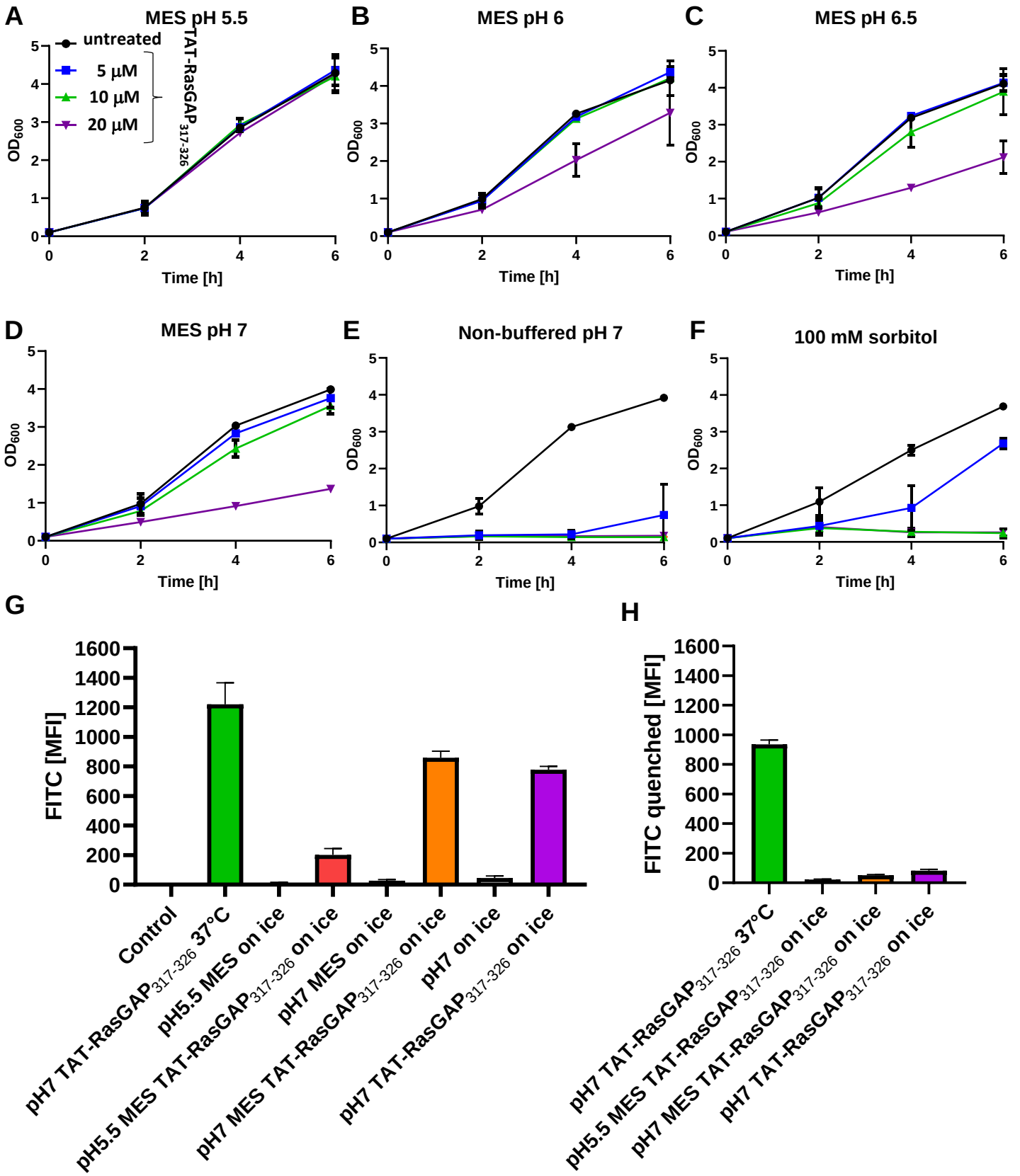

Figure 2: Low pH and high buffering capacities of medium differently affect activity of TAT-RasGAP$_{317-326}$. A-F) *E. coli* MG1655 was grown overnight at 37°C in LB medium containing 100 mM MES at the indicated pH (A-D), non-buffered LB at pH 7 (E) or LB supplemented with 100 mM sorbitol (F). Cultures were diluted to 0.1 OD_{600} in the same medium and grown one hour at 37°C before addition or not of the indicated concentrations of TAT-RasGAP$_{317-326}$. OD_{600} was measured at the indicated time points. **G)** *E. coli* MG1655 were treated as in (A-F) and FITC-labelled TAT-RasGAP$_{317-326}$ was added either at 37°C or on ice. Fluorescence was then quantified using flow cytometry. MFI: geometric mean of fluorescence intensity. Control are unlabeled bacteria. H) Extracellular FITC signal after quenching with trypan blue.

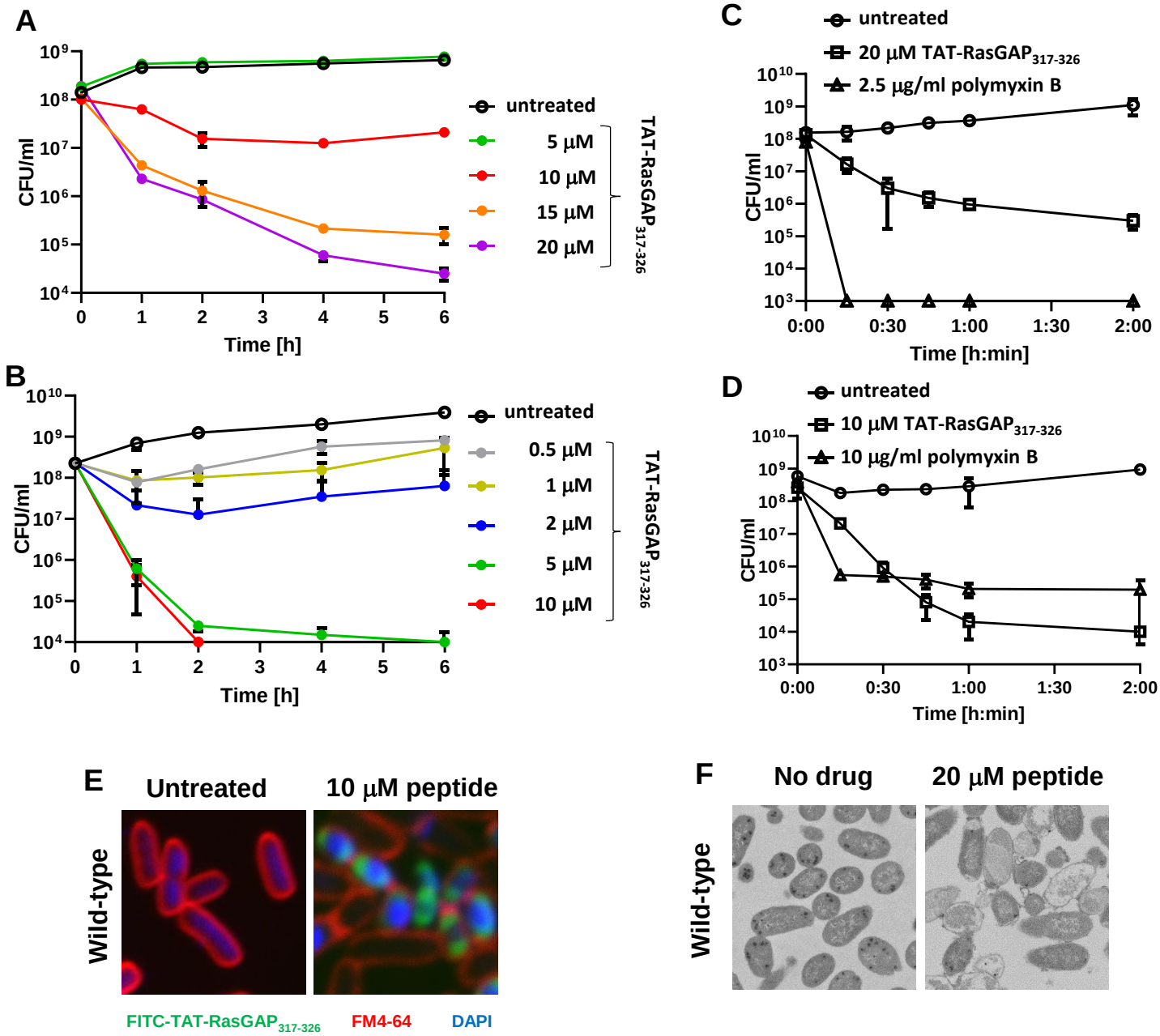

Figure 3: TAT-RasGAP$_{317-326}$ is bactericidal against *E. coli* and *P. aeruginosa*. A-D) Overnight cultures of *E. coli* MG1655 in LB (A-B) and *P. aeruginosa* PA14 in BM2 Mg^{low} (C-D) were diluted to 0.1 OD_{600}. Peptide was added at the indicated concentrations 1 hour after dilution. Samples were taken at the indicated time points, serially diluted 10-fold in fresh LB and plated on LB agar plates. Number of colony forming unit per ml (CFU/ml) of original culture was calculated. **E)** *E. coli* MG1655 strain was incubated for one hour with or without 10 µM FITC-labelled TAT-RasGAP$_{317-326}$. The bacterial sample was then labelled with 5 µg/ml FM4-64 and fixed with 4% paraformaldehyde solution. Incubation with DAPI was subsequently performed. Pictures were taken with a Zeiss LSM710 confocal microscope and analyzed using ImageJ software. **F)** *E. coli* bacteria treated as in (E) were fixed using glutaraldehyde and prepared for electron microscopy as described in Material and Methods section. Samples were imaged using transmission electron microscopy. Images were analyzed using ImageJ software.

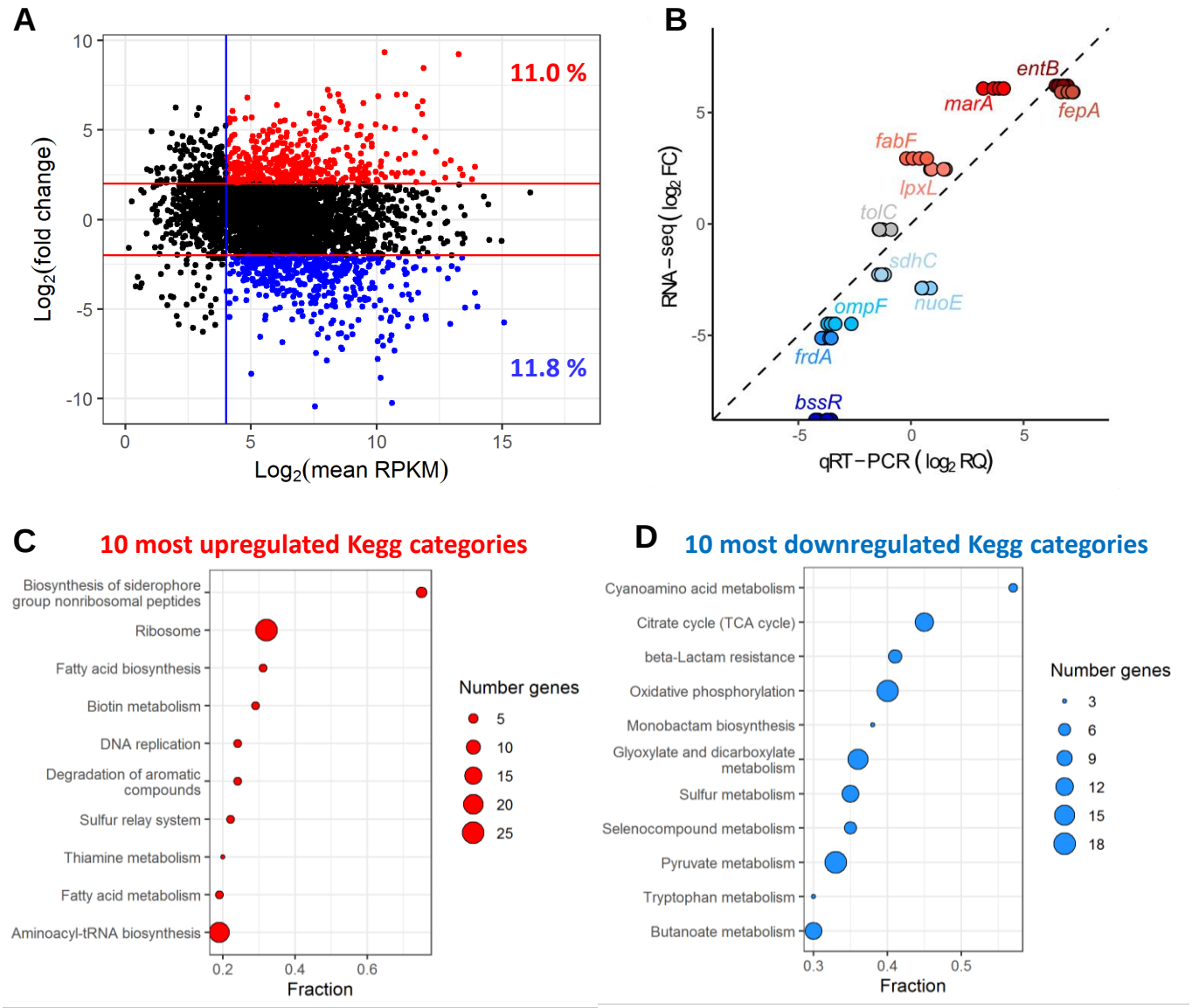

Figure 4: TAT-RasGAP$_{317-326}$ remodels the transcriptional landscape of *E. coli*. RNA-seq analysis was performed on E. coli grown for 1h in the presence or absence of TAT-RasGAP$_{317-326}$. **A**) MA-plot of the average gene expression (x-axis, RPKM: read per kilobase million) vs the differential expression (y-axis). Threshold for gene expression is indicate with the blue horizontal line. The red lines indicate the limits for upregulated (red dots) and downregulated (blue dots) genes. **B**) Correlation between RNA-seq (log_2 Fold Change) and qRT-PCR (log_2 Relative Quantification) differential expression for a set of genes. **C-D)** Fraction of KEGG pathway genes that are upregulated (B) or downregulated (C) after treatment with TAT-RasGAP$_{317-326}$. Dot size indicates the number of genes in the selection.

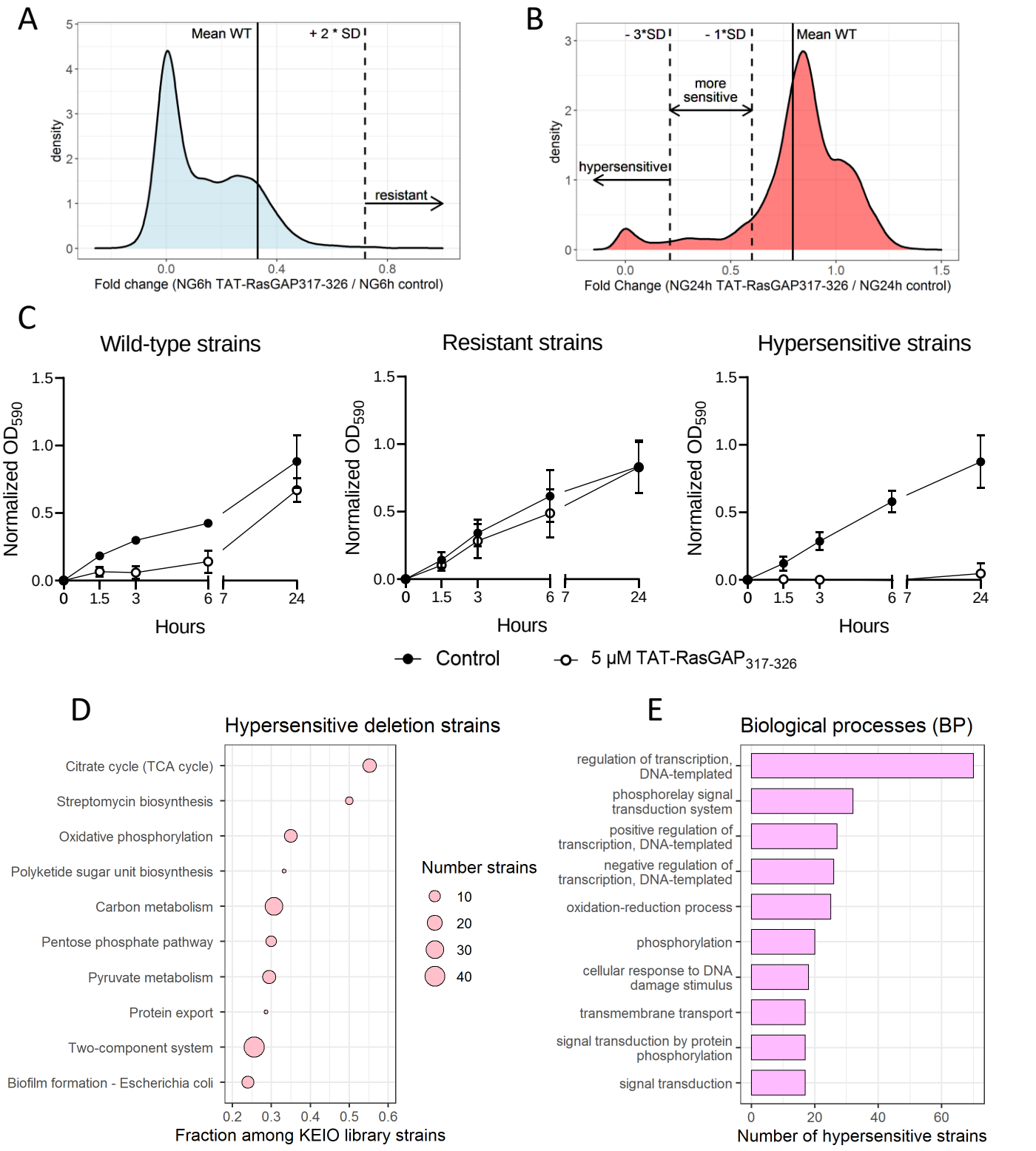

Figure 5: Selection of hypersensitive and resistant *E. coli* deletion strains from KEIO collection. Single gene deletion strains were grown in LB medium with or without 5 µM TAT-RasGAP$_{317-326}$ and OD_{590} was measured at 0, 1.5, 3, 6, and 24 hours. **A-B**) Distribution of the fold change of the normalised growth (NG) with TAT-RasGAP$_{317-326}$ vs without peptide at 6h (A) and 24h (B). The mean of the wild-type strain and the standard deviation (SD) are indicated with the vertical solid and dashed lines, respectively. Arrows indicate the strains selected as resistant, hypersensitive and more sensitive. **C**) Growth curves of wild-type (n=270), hypersensitive (n=356) and resistant (n=20) strains. Data are mean ± SD. **D**) Top 10 most represented KEGG pathways among hypersensitive strains. The number of hypersenstive strains in each pathway was normalised to the number of KEIO collection strains in the corresponding pathway. **E**) Biological processes GO term enrichment analysis with the 10 most represented terms among the hypersensitive strains.

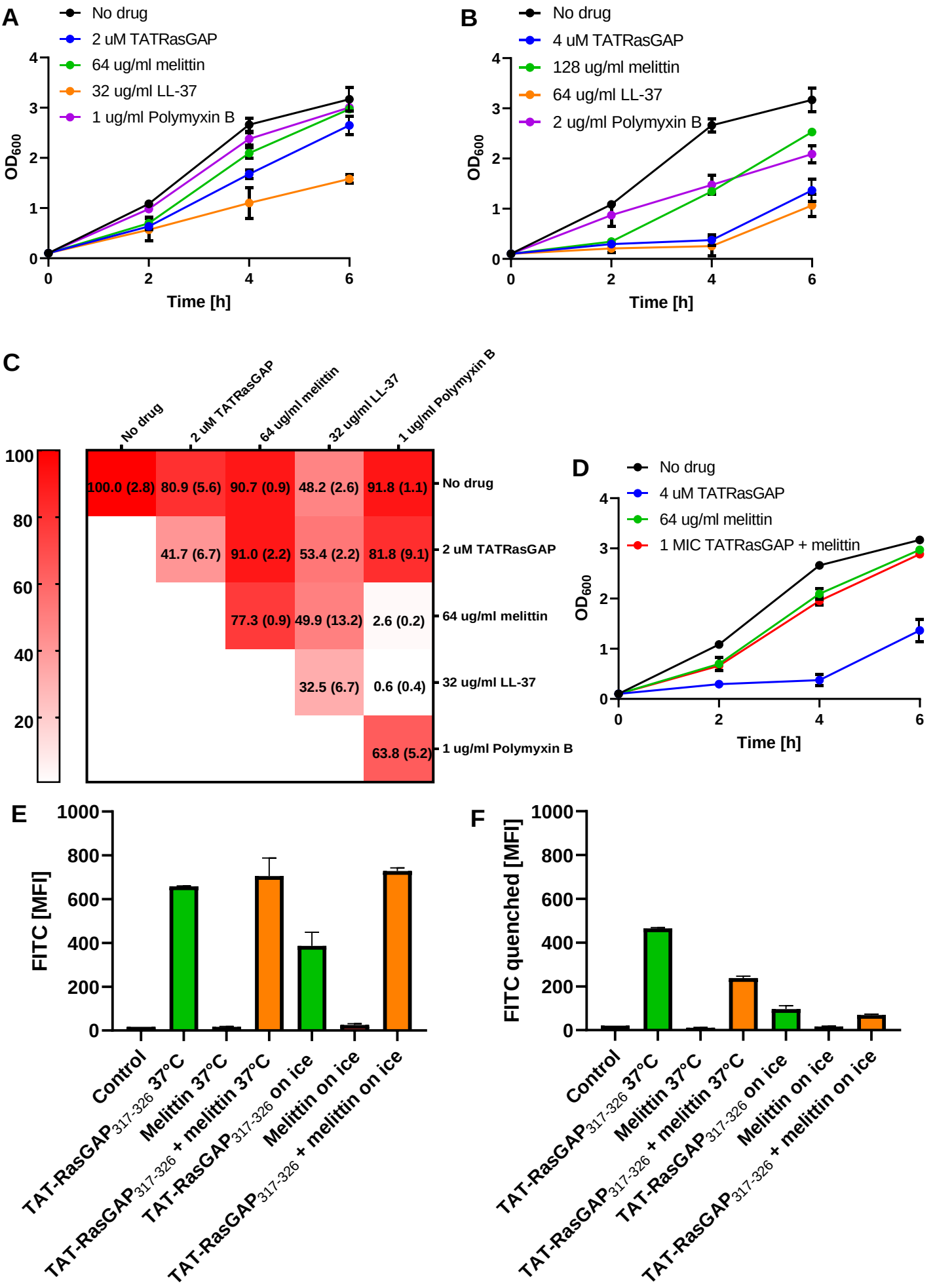
A
No drug
2 uM TATRasGAP
64 ug/ml melittin
32 ug/ml LL-37
1 ug/ml Polymyxin B
OD600
Time [h]
B
No drug
4 uM TATRasGAP
128 ug/ml melittin
64 ug/ml LL-37
2 ug/ml Polymyxin B
OD600
Time [h]
C
No drug
2 uM TATRasGAP
64 ug/ml melittin
32 ug/ml LL-37
1 ug/ml Polymyxin B
100.0 (2.8)
80.9 (5.6)
90.7 (0.9)
48.2 (2.6)
91.8 (1.1)
41.7 (6.7)
91.0 (2.2)
53.4 (2.2)
81.8 (9.1)
77.3 (0.9)
49.9 (13.2)
2.6 (0.2)
32.5 (6.7)
0.6 (0.4)
63.8 (5.2)
D
No drug
4 uM TATRasGAP
64 ug/ml melittin
1 MIC TATRasGAP + melittin
OD600
Time [h]
E
FITC [MFI]
Control
TAT-RasGAP317-326 37°C
Melittin 37°C
TAT-RasGAP317-326 + melittin 37°C
TAT-RasGAP317-326 on ice
Melittin on ice
TAT-RasGAP317-326 + melittin on ice
F
FITC quenched [MFI]
Control
TAT-RasGAP317-326 37°C
Melittin 37°C
TAT-RasGAP317-326 + melittin 37°C
TAT-RasGAP317-326 on ice
Melittin on ice
TAT-RasGAP317-326 + melittin on ice

Figure 6: TAT-RasGAP$_{317-326}$ shows no synergism with melittin, LL-37 and polymyxin B. *E. coli* MG1655 was grown overnight, diluted to 0.1 OD_{600}, and grown further during one hour before addition of the indicated AMPs. OD_{600} was measured at 2, 4 and 6h. For each AMP, two concentrations were tested: **(A)** a non-inhibitory concentration and **(B)** an inhibitory concentration corresponding to twice that of panel A. **C)** Combinations of AMPs were then tested and growth at 6h was expressed as percentage of growth compared to an untreated control. **D)** Sub-inhibitory concentration of melittin interfered with TAT-RasGAP$_{317-326}$ activity. Indicated AMPs were added and OD_{600} was measured as in (A). **E)** Bacteria were treated as in (A), but FITC-labelled TAT-RasGAP$_{317-326}$ was added and flow cytometry was performed in the indicated conditions. MFI: geometric mean of fluorescence intensity. Control are unlabeled bacteria **F)** Extracellular fluorescence after quenching with trypan blue.

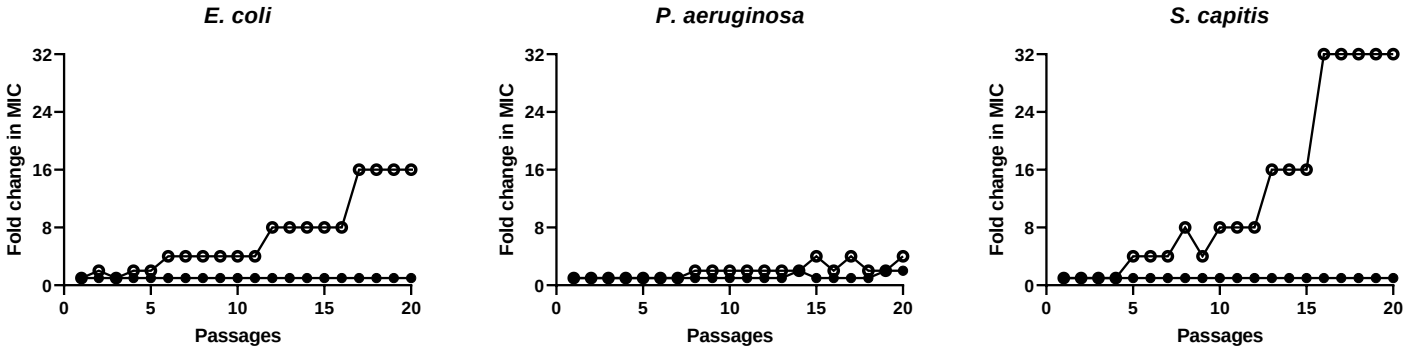

Figure 7: Bacterial resistance against TAT-RasGAP$_{317-326}$ appears after selection with subinhibitory concentrations of peptide. The indicated strains were incubated in presence or absence of 0.5 MIC of TAT-RasGAP$_{317-326}$. Cultures were then diluted each day in medium containing either the same concentration of the peptide or double the concentration. Once bacterial growth was detected in the culture exposed to an elevated concentration of the peptide, the process was repeated thereby exposing the bacterial culture to sequentially increasing concentrations of peptide for a total of 20 passages. MIC of each passage was then measured and is presented as a fold change compared to the MIC of the original strain.

.